A retrospective evaluation of automated optimization of deep brain stimulation parameters

Johannes Vorwerk[a], Andrea A. Brock[b], Daria N. Anderson[a,c], John D. Rolston[b,c], Christopher R. Butson[a,b,c,d,e,*]

[a]*Scientific Computing & Imaging (SCI) Institute, University of Utah, Salt Lake City, UT, USA*
[b]*Department of Neurosurgery, Clinical Neurosciences Center, University of Utah, Salt Lake City, UT, USA*
[c]*Department of Biomedical Engineering, University of Utah, Salt Lake City, UT, USA*
[d]*Department of Psychiatry, University of Utah, Salt Lake City, UT, USA*
[e]*Department of Neurology, University of Utah, Salt Lake City, UT, USA*

Abstract

Background: The automatic determination of optimal deep brain stimulation (DBS) parameters is of great importance to improve the stimulation control of the classic quadripolar and the increasingly popular segmented DBS leads. Several algorithms to fulfill this goal have been presented recently, but few data exist validating the computationally predicted settings against patient data.
Objective: We perform a retrospective analysis of a proposed optimization algorithm to show that its application in practice has the potential to lead to an equal or better stimulation of the target region as manual programming, while reducing the time effort for programming sessions.
Methods: For three patients (five electrodes) diagnosed with essential tremor, we derived the voltage thresholds at which side effects occur for each contact during the initial programming session. Based on these voltage thresholds, we automatically derived optimal stimulation settings using an approach that can be applied in clinical practice.
Results: We observe a high degree of agreement between the findings of manual programming and the results of the optimization algorithm, with the algorithm predicting a clinically utilized electrode contact in 80% of the cases. Additionally, the optimized stimulation settings lead to the activation of an equal or larger volume fraction of the target compared to the manually determined settings in all cases.
Conclusions: Our results validate the automatic determination of optimal DBS settings against patient data, as we find that the optimization results reliably agree with the manually determined optimal stimulation settings. Thereby, we

*Corresponding author
Email addresses: `jvorwerk@sci.utah.edu` (Johannes Vorwerk), `butson@sci.utah.edu` (Christopher R. Butson)

demonstrate the feasibility and benefit of applying this algorithm in clinical practice.

Keywords: neuromodulation, essential tremor, computational modeling, thalamus, ventral intermediate nucleus

---

1. Introduction

Deep brain stimulation (DBS) has been established as a treatment for movement disorders, such as Parkinson's disease and essential tremor [1, 2], and is currently evaluated as a treatment for a variety of other neurological disorders. Depending on a patient's diagnosis and symptoms, DBS leads are implanted in specific anatomical targets in the brain during a stereotactic surgery. A common DBS target to treat essential tremor is the ventral intermediate nucleus (VIM) [3, 4, 5], which was also chosen for the patients included in our study.

A few weeks after the implantation of the DBS lead, an initial programming session is performed to start the treatment. Commonly, a comprehensive monopolar review is performed during this session, in which the clinican tries to find optimal stimulation settings for the specific patient by varying the stimulation parameters. Parameters that can be varied are active lead contact(s), stimulation voltage, pulse width, and pulse frequency. For each contact of the DBS lead, the settings with beneficial effects and the thresholds at which side effects occur for cathodic-first charge-balanced pulses are determined. This monopolar review may require several hours of programming time [6, 7]. If the treatment results are not satisfactory, an exploration of alternative stimulation configurations, such as bipolar stimulation settings, may be performed [8, 9]. For most patients, multiple follow-up programming sessions are necessary to refine the stimulation parameters, leading to a significant time effort for both the patient and the caregivers. The time expended for the manual programming of DBS patients is expected to grow exponentially with the emerging use of DBS leads that have an increased number of (smaller) contacts than the previously standard quadripolar leads. Such leads are promising better treatment outcomes due to their improved field-shaping abilities [10, 11, 12, 13, 14, 15].

To decrease programming times and to fully capitalize on the effects of these novel lead models, different research groups have presented algorithms for an automatic determination of optimal DBS settings [16, 17, 18, 19, 20]. Whereas these algorithms have been positively validated in simulation studies, few data exist validating the computationally predicted stimulation settings against clinical data.

In this study, we perform a retrospective evaluation of the algorithm presented by Anderson et al. [20]. Based on specific target and avoidance regions, the algorithm performs an optimization that maximizes stimulation of the target region and keeps the stimulation of the avoidance regions below a certain threshold. In our study, we expanded this optimization algorithm to additionally enforce the efficiency of the stimulation, so that activation of lead contacts

Table 1: Patient overview. t_{lead} indicates the time between the initial programming session and lead placement, t_{IPG} the time between the initial programming session and IPG placement (w = weeks, d = days).

	Sex	Age	Hemisphere	ET impairment (off medication)	t_{lead}	t_{IPG}
P1	W	53	Bilateral	upper extremities	2 w	3 d
P2	M	64	Left	upper extremities, disability of RH	5.5 w	3.5 w
P3	M	71	Bilateral	upper extremities, progressive	5.5 w	5.5 w

that do not stimulate the target region is efficiently suppressed. To perform our retrospective evaluation, we utilized detailed notes of stimulation settings and observed side effects taken during the initial programming session of multiple patients with VIM DBS for essential tremor.

2. Material and methods

2.1. Patient cohort and imaging

We obtained data from three DBS patients who were diagnosed with essential tremor. All patients gave written informed consent and all procedures were approved by the independent research board (IRB) of the University of Utah (#44402). Patient details are listed in Table 1. All patients were implanted with Medtronic 3387 leads. For the evaluation of the optimization results, we refer to these patients as PXY, where X is the patient id between 1 and 3, and Y the stimulation site, i.e., either L for left or R for right.

For all patients, preoperative MP2RAGE T1-weighted (T1w-) scans (voxel size = 1 x 1 x 1 mm, FOV = 255 x 255 x 176 mm) were acquired on a 3 T MR scanner (MAGNETOM Prisma 3.0 T, Siemens Healthcare, Erlangen, Germany). Additionally, multi-shell diffusion spectrum (DS-) MRI scans with 64 directions for each b-value (voxel size 1.49 x 1.49 x 1.5 mm, FOV = 250 x 250 x 139.5 mm, b-values = 700, 2000, 3000 s/mm^2) and volumes with flat diffusion gradient (b = 0 s/mm^2) for both regular and inverted phase encoding direction were acquired. The DSI volumes were corrected for eddy currents, head motions, and susceptibility artifacts using ACID (http://www.diffusiontools.com; [21, 22]) and resampled to an isotropic voxel size of 1 x 1 x 1 mm.

Computed tomography (CT) images were acquired (voxel size = 0.75 x 0.75 x 1 mm) on an AIRO Mobile CT system (Brainlab AG, Feldkirchen, Germany) to reconstruct the lead positions.

2.2. DBS programming notes

During each patient's initial programming session, we recorded the voltages for monopolar cathodic-first charge-balanced stimulation (hereafter referred to as cathodic stimulation) at which beneficial or side effects occurred for each contact. At the end of the programming session, we noted the clinically used settings, i.e., the settings (contact, stimulation voltage, pulse width and frequency) that led to an optimal treatment for the specific patient and the settings that were considered as alternatives.

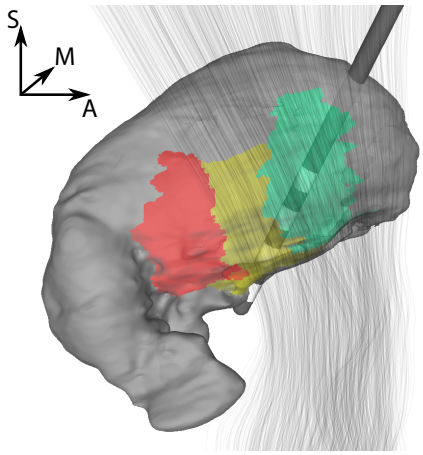

Figure 1: Surface visualization of lead placement relative to thalamus (gray) and IC (gray lines) for P1R. Colored are selected subregions of the thalamus (from left to right VPL - red, VIM/VLpv - yellow, VLa - green).

For each patient, the highest voltage for each contact that did not lead to side effects and the clinically optimal and alternative setting are listed in Table 2. Given that only cathodic-first stimulation is considered in this study, we indicate only the contact and the absolute value of the voltage throughout the manuscript.

2.3. Selection of target and avoidance regions for the optimization algorithm

To apply the optimization algorithm, it is necessary to select target regions for which the stimulation is maximized and regions of avoidance for which the stimulation is kept below a certain threshold to minimize side effects. We selected the VIM as the target region and the ventral posterolateral nucleus (VPL) and the internal capsule (IC) as avoidance regions (see, e.g., Fig. 1, Krauth et al. [23], Bakay [24, Fig. 11.2]), as stimulation of VPL and IC can lead to parasthesias and dysarthria or motor contractions, respectively [25].

2.4. Atlas registration and fiber tractography

Preoperative imaging was used to obtain individual segmentations as representations of the target and avoidance regions VIM, VPL, and IC as follows:

The T1w-MRIs were nonlinearly registered to the "MNI ICBM 152 nonlinear 6th Generation Average Brain" (MNI-ICBM152) [26] using ANTs [27]. For this average brain, surface segmentations of the posteroventral part of the ventrolateral nucleus (VLpv), which largely corresponds to the VIM in Jones nomenclature (see, e.g., Bakay [24, Fig. 11.2]), and the VPL were obtained from the Morel atlas [23]. Patient individual surface segmentations of VLpv and VPL were obtained by applying the inverse of the nonlinear transform from patient images to the MNI-ICBM152 average brain to the surface segmentations.

Tractography of the internal capsule (IC) was performed using DSIStudio (dsi-studio.labsolver.org) for each patient and hemisphere [28]. A seed region to generate IC tractography was manually segmented based on the fractional anisotropy.

2.5. Finite element simulation of DBS

We used the finite element method (FEM) to solve the bioelectric field problem of DBS for the Medtronic 3387 lead [29]. For each patient, we obtained a triangular surface mesh of the brain's surface with FSL (https://fsl.fmrib.ox.ac.uk) and a triangular surface mesh of the Medtronic 3387 lead. Based on these surface meshes, a tetrahedral volume mesh was generated using TetGen [30], from which the elements inside the lead were clipped. Furthermore, we included the nodes at which we later evaluated the electric potential u as mesh vertices. These nodes are distributed on a regular grid with a size of 20 x 20 x 30 mm and an internode distance of 0.2 mm around the center of the lead.

We solved the bioelectric field problem with a linear FEM using SCIRun 5 (http://www.sci.utah.edu/cibc-software/scirun.html). We chose a conductivity of 0.2 S/m for the brain volume. Active contacts were modeled by imposing a Dirichlet boundary condition set to the stimulation voltage at the contact surface, a Dirichlet boundary condition of 0 V at the brain surface, and a homogeneous Neumann boundary condition at the insulating lead shaft. The passive contacts were modeled as linked nodes.

Due to the linearity of the problem, it is sufficient to solve the bioelectric field problem for a unit voltage of -1 V at each contact while all other contacts are passive. For each solution of the electric potential, we computed the Hessian matrix H, which is needed for the optimization algorithm described in Section 2.6, at the predefined set of nodes around the lead. The voltage distributions $u_{\mathbf{c}}$ and Hessian matrices $H_{\mathbf{c}}$ for general stimulation voltages $\mathbf{c} = (c_0, c_1, c_2, c_3)$ follow by linear combination.

2.6. Optimization algorithm

We applied a modification of the optimization algorithm presented by Anderson et al. [20]. The algorithm relies on the activating function as a predictor for neuronal activation [31, 32, 33, 34]. To easily obtain the activating function, we numerically calculated the Hessian matrix of partial second derivatives of the electric potential $u_{\mathbf{c}}$:

$$H_{u_{\mathbf{c}}}(\mathbf{x})_{i,j} = \frac{\partial u_{\mathbf{c}}(\mathbf{x})}{\partial x_i \partial x_j} \text{ for } \mathbf{x} \in \Omega, \quad i,j = 1,2,3. \tag{1}$$

Varying the approach of Anderson et al. [20], we used the value of the second derivative of the electric field in a direction perpendicular to the shaft of the DBS electrode to estimate activation of both the target and avoidance region, which resembles the distribution of neurons used to compute the volume of tissue activated (VTA) [35, 36]. Based on the Hessian matrix, the activation at

a position $\mathbf{x}$ with a corresponding direction $\mathbf{n}_p$ perpendicular to the electrode shaft can be computed as

$$a_p(\mathbf{x}, \mathbf{c}) = \mathbf{n}_p^t(\mathbf{x}) H_{u_\mathbf{c}}(\mathbf{x}) \mathbf{n}_p(\mathbf{x}) \text{ for } \mathbf{x} \in \Omega. \tag{2}$$

Accordingly, the objective function to measure activation of the target region, $\Omega_{\text{VIM}} \subset \Omega$, is defined as

$$f(\mathbf{c}) = \int\limits_{\Omega_{\text{VIM}}} a_p(\mathbf{x}, \mathbf{c}) \, \mathrm{d}x. \tag{3}$$

We introduced an additional regularization term to the optimization functional to favor stimulation settings with a higher efficiency, i.e., a better ratio between stimulation of target and nontarget regions, by penalizing stimulation of the nontarget volume:

$$g(\mathbf{c}) = \int\limits_{\Omega - \Omega_{\text{VIM}}} a_p(\mathbf{x}, \mathbf{c})^2 \, \mathrm{d}x. \tag{4}$$

For the avoidance of the VPL, we kept the value of a_p below a threshold α in the region Ω_{VPL}. For the avoidance of the IC, we make use of the fiber orientations obtained from tractography. We denote the fiber orientation at position $\mathbf{x}$ by $\mathbf{n}_f(\mathbf{x})$ and define a_f according to (2) with $\mathbf{n}_p$ replaced by $\mathbf{n}_f$. As for the avoidance of the VPL, a_f is kept below α to avoid stimulation of the IC. We also refer to α as sensitivity parameter hereafter.

With these constraints, our optimization problem can be formulated as

$$\begin{aligned} &\text{maximize } f(\mathbf{c}) - \lambda g(\mathbf{c}) \\ &\quad \text{subject to } 0 \leq c_i \leq c_{max}, \\ &\qquad a_p(\mathbf{x}, \mathbf{c}) \leq \alpha \text{ for } \mathbf{x} \in \Omega_{\text{VPL}}, \\ &\qquad a_f(\mathbf{x}, \mathbf{c}) \leq \alpha \text{ for } \mathbf{x} \in \Omega_{\text{IC}}. \end{aligned} \tag{5}$$

The algorithm was evaluated only for optimization of cathodic-first stimulation so far. Thus, the condition $0 \leq c_i$ restricts the resulting stimulation to be cathodic, as we set $c_i = -1\,\text{V}$ in our FEM simulation. c_{max} indicates the upper threshold for the stimulation voltage. α is a regularization parameter that determines how much weight is given to the efficiency of the stimulation in the optimization. We used $\lambda = 0.001$ in this study.

In practice, the integrals in the expressions for f and g turn into summations over all (grid) points in the respective region. We solved the resulting optimization problem using the python package cvxopt (cvxopt.org).

2.7. Retrospective determination of optimal stimulation settings

In theory, the sensitivity parameter α represents the value of the activating function above which neuron firing occurs as a result of the stimulation.

Table 2: Clinically obtained voltage thresholds from monopolar review (bold face marks clinical choices, underlined marks optimal choice) and optimization results (bold face marks voltage maximum).

Patient #		α [mV/mm^2]	C0 [V]	C1 [V]	C2 [V]	C3 [V]
P1R	Clinical threshold		0.60	0.80	0.80	**<u>2.50</u>**
	Optimization	15	0.00	0.00	0.78	**1.31**
P1L	Clinical threshold		0.50	0.80	**<u>1.50</u>**	1.60
	Optimization	104	0.08	0.00	**1.50**	0.00
P2L	Clinical threshold		0.70	**1.50**	**<u>1.50</u>**	1.60
	Optimization	41	**0.70**	0.49	0.19	0.03
P3R	Clinical threshold		0.50	0.50	**<u>1.50</u>**	**1.60**
	Optimization	28	0.00	0.50	**1.10**	0.80
P3L	Clinical threshold		0.70	**<u>2.00</u>**	**3.00**	3.80
	Optimization	31	0.59	1.98	**2.21**	0.82

However, although approximate values for this parameters can be found using neuron simulations [37, 35, 38], the exact value at which side effects occur is not known in practice.

Instead, to retrospectively apply the optimization algorithm, we used the thresholds that were obtained during the monopolar review (see Sec. 2.2). These values provide the voltage limits up to which a stimulation of each contact of the DBS lead is possible without causing side effects. To obtain the optimal stimulation settings within these voltage limits, we incrementally increased the parameter α in steps of $0.1\,\mathrm{mV/mm^2}$ until the voltage threshold at one contact was exceeded. The last optimization result for which all voltages fell below the thresholds was selected as our optimal stimulation setting.

3. Results

Table 2 shows the voltage thresholds obtained during the monopolar review (line "Clinical threshold"), the clinically selected settings, and the result of the optimization algorithm (line "Optimization").

The results of the optimization algorithm show good agreement with the outcome of the monopolar review. For all patients except P2L, the contact with the maximal voltage computed by the optimization algorithm corresponds to a contact that was found to be clinically effective during the monopolar review. In three of these cases (except P3L), the contact assigned the highest voltage by the optimization algorithm is the contact that was manually found to lead to optimal results.

As a measure of the efficiency of the stimulation, we visualize the percentage of the target volume Ω_{VIM} for which a_p is above the sensitivity α for both the optimized stimulation settings and the clinically determined settings in Figure 2a. For each patient and hemisphere, the sensitivity parameter α was determined according to Table 2, which means that the assumed sensitivity varies for different patients and hemispheres. The depicted measure should not be

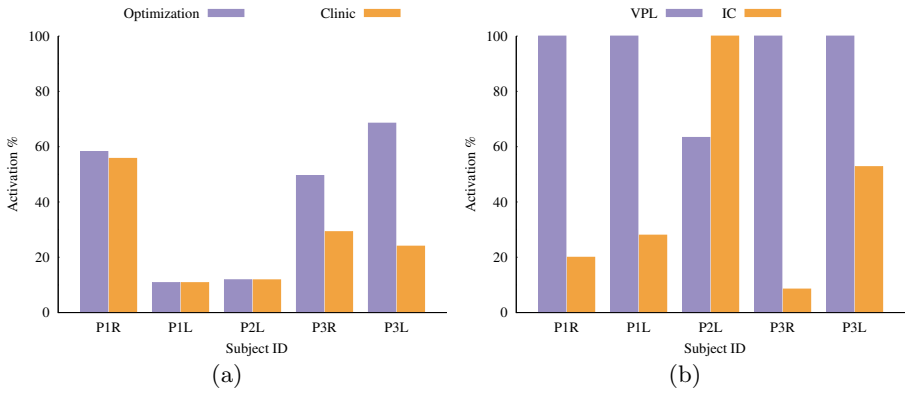

Figure 2: a) Target activation, measured in % of Ω_{VIM} for which a_p is above the sensitivity α, for the result of the optimization algorithm (purple) and clinically chosen stimulation setting (orange). b) Maximal activation a_p and a_f of VPL (purple) and IC (orange), respectively, relative to sensitivity parameter α (see Tab. 2).

confused with the actual stimulation of the target. Figure 2a shows that the optimization algorithm leads to a stimulation that is at least as effective as the clinically determined settings in all cases. For P3R and P3L the stimulation of the target could be clearly improved by using the algorithm-derived settings. For P1R, the optimized stimulation setting slightly improves the stimulation of the VIM, despite a clearly lower maximal stimulation voltage of 1.3 V compared to 2.5 V for the clinically determined setting.

To understand which avoidance condition is most influencing the optimization result, we visualize the maximum of the activation a_p and a_f of VPL and IC, respectively, relative to the sensitivity parameter α chosen for the specific electrode (see Tab. 2) in Figure 2b. If a_p or a_f is at 100%, the stimulation of the respective avoidance region, i.e., VPL or IC, limits the stimulation, as the sensitivity threshold α would be exceeded at higher stimulation voltages in this avoidance region and side effects might occur. These results show that in all cases except for P2L, the avoidance of the VPL is the dominating condition. In these cases, the contacts that lead to the best stimulation of the VIM stimulate the VPL more than the IC.

Next, we analyze three examples in more detail. For P1R and P1L, the optimization algorithm led to stimulation settings that closely fit the clinically chosen settings with a nearly identical activation of the VIM at 50% and 10%, respectively. P2L is the only evaluated case in which optimization result and clinically determined stimulation settings clearly differ. For both stimulation settings for P2L, the activation of the VIM is at a low level of about 10%, but whereas C2 was manually selected for stimulation, the maximal voltage is applied at C0 for the optimization result.

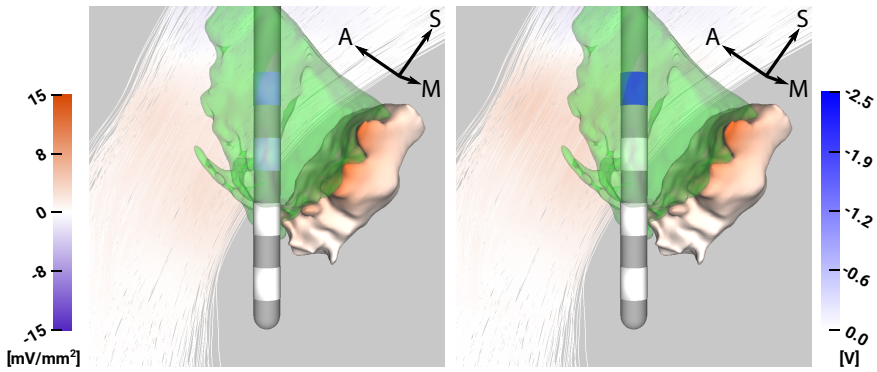

(a) (b)

Figure 3: P1R - Visualization of VIM (green), a_p and a_f mapped on VPL and IC (left colorbar in mV/mm^2) and stimulation voltage mapped on lead contacts (right colorbar in V), respectively, for a) optimization result and b) monopolar stimulation with 2.5 V at C3.

3.1. Analysis of P1R

Figure 3 shows that both C2 and C3 are inside the VIM (green), thus similarly contributing to the target stimulation. However, C2 is closer to the VPL than C3, whereas the IC is relatively distant from both of these contacts. C0 and C1 are both (mostly) outside the VIM, thereby stimulating the VIM less efficiently than C2 and C3. In line with these considerations, C2 and C3 are selected as active contacts by the algorithm, with a stronger voltage assigned to C3, which is more distant from the VPL. Figure 3a shows that the sensitivity α is reached in the VPL for the optimization result, whereas the stimulation of the IC is clearly below the threshold. In line with the optimization result, we also see a stronger stimulation of the VPL than the IC for the clinically determined stimulation setting (Fig. 3b). Furthermore, the clinically determined stimulation setting leads to a stronger stimulation of the VPL than the optimization result, but the stimulation of the VIM is slightly worse (Fig. 2).

3.2. Analysis of P1L

For P1L, we find that C2 is fully contained in the lateral part of the VIM, whereas C1 is found to be inside both the target and avoidance region (Fig. 4). C0 lies inferior to the VIM partially inside the avoidance region, and C3 lies superior to the VIM. Thus, C1 and C2 show the strongest contribution to the target stimulation; C0 and C1 lead to a strong stimulation of the VPL. All contacts lead to only a low stimulation of the IC. These considerations explain why the optimization algorithm leads to an exclusive activation of C2 – the other contacts are either in the avoidance region (C0, C1) or outside the VIM (C0, C3).

3.3. Analysis of P2L

P2L was the only case in which the optimization algorithm did not assign the maximal voltage to a clinically used contact. Using the algorithm, the

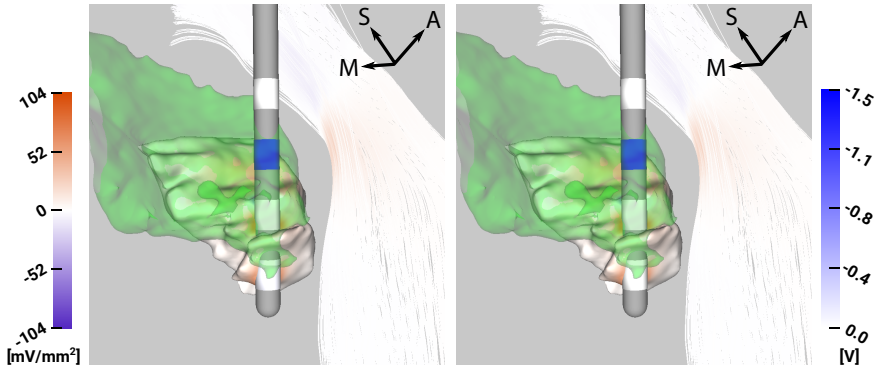

(a) (b)

Figure 4: P1L - Visualization of VIM (green), a_p and a_f mapped on VPL and IC (left colorbar in mV/mm^2) and stimulation voltage mapped on lead contacts (right colorbar in V), respectively, for a) optimization result, b) monopolar stimulation with 1.5 V at C2.

maximal voltage was assigned to C0, a contact for which finger parasthesias were observed at 0.8 V during monopolar review, whereas C1 proved to be best at reducing tremor. However, C1 also produced transient parasthesias at 1.5 V and ataxia with finger-nose-finger testing at 1.8 V. In fact, a bipolar setting was manually chosen as the optimal stimulation, which was outside the scope of our evaluation.

Figure 5 visualizes the clinically chosen stimulation and the optimization result for P2L. The lead is placed frontal to the VIM, with C0 and C1 being partially contained in this region. Accordingly, we find that C0 and C1 contribute strongest to the target stimulation at an approximately equal level. We further find that C0 leads to the weakest stimulation of the avoidance regions; the IC receives a much stronger stimulation through the other contacts.

The visualization of the clinically selected monopolar stimulation, i.e., stimulation at contact C1 with 1.5 V, shows a much stronger stimulation of the IC than the optimized stimulation setting. The maximal value of a_f is about 37 for this setting, whereas it is 9.5 for the optimization result.

These results suggest that the representation of the avoidance regions, i.e., the atlas-based segmentation of VIM and VPL and the tractography of the IC, might be inaccurate for this patient. Whereas we ensured that the boundary of the thalamus is accurately segmented, it is not easy to verify the segmentation of the thalamic nuclei due to the low contrast within thalamus. Alternative explanations, such as the possible need to add additional avoidance regions, are unlikely. With our current computational model, there exists no obvious explanation why a much lower side effect threshold was found for C0 compared to C1.

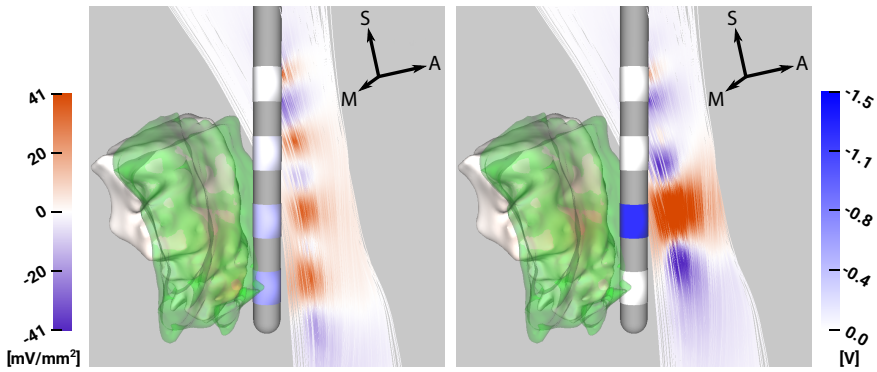

(a) (b)

Figure 5: P2L - Visualization of VIM (green), a_p and a_f mapped on VPL and IC (left colorbar in mV/mm^2) and stimulation voltage mapped on lead contacts (right colorbar in V), respectively, for a) optimization result and b) monopolar stimulation with 1.5 V at C1.

4. Discussion

In this study, we performed a retrospective evaluation of an algorithm for the optimization of DBS settings. Our results showed good agreement between the optimization result and clinically determined parameters; in 80% of the cases, the optimization algorithm assigned the strongest stimulation voltage to clinically used contacts. In all cases, the stimulation of the target achieved by the optimization algorithm was at least equal to the clinically determined settings; in three of these cases, the stimulation was improved.

4.1. Impact

The results obtained in this study are an important validation of the applied optimization algorithm, and they encourage its application in clinical practice. Our results indicate that VPL and IC are appropriate avoidance regions for the automated optimization of VIM stimulation. The results furthermore validate our choice of the activating function, implemented in the avoidance measures a_p and a_f, as a predictor for neural activation.

The approach that we chose in this study to obtain the sensitivity parameter α, is the same that we foresee will be used in clinical practice. The clinician starts to program the patient with a low value of α. Subsequently, α gets incrementally increased, and the patient programming gets updated with a new optimization result. This step is repeated until side effects occur, whereupon a programming setting for the previous lower value of α is chosen. Our work shows that this procedure leads to equivalent, if not better, stimulation settings as a classical monopolar review.

Most centers explore the space of possible stimulation parameters by first evaluating each contact individually in a monopolar review and then using clinical intuition and heuristics to refine their results. This method, since it relies

on intuition, is challenging to teach and not guaranteed to find an optimal result. As novel electrode geometries and configurations continue to proliferate, the parameter space for DBS programming grows exponentially, and manual exploration of the parameter space will become even more complicated. Our proposed semiautomated method improves upon this manual process by reducing the stimulation voltage or current on each electrode contact to a single parameter, α, which incorporates all electrode contacts. The sensitivity parameter α is varied in a stepwise fashion and corresponds to contact selection optimized to stimulate the target region and avoid regions that can generate side effects (like VPL and IC, in the case of VIM stimulation). This method is able to reduce the parameter space by utilizing the pre- and postoperative imaging data that is functionally ignored during a monopolar review. The necessity of varying α (vs. directly computing stimulation settings) arises from our inability to perfectly map models of stimulated tissue to perception (i.e., side effects) at the level of an individual patient, although this limitation may ultimately recede as our modeling and imaging methods improve.

4.2. Related work

The algorithm applied in this study is based on the work of Anderson et al. [20]. Through the addition of the functional g as defined in (4), we were able to modify this algorithm to also enforce an efficient stimulation and maximize stimulation of the target region, minimize stimulation of other brain regions, and stay below the side-effect threshold in the avoidance regions simultaneously. The balance between optimal stimulation of the target and power efficient stimulation can be regulated through the choice of the parameter λ. Our results justify our choice of λ, leading to stimulation settings in which maximally two contacts were assigned with a significant stimulation voltage, in combination with a better stimulation of the VIM than the clinically chosen stimulation settings.

The objective function that was applied here is comparable to the one proposed by Wagner et al. [39] for transcranial direct current stimulation (tDCS) or by Peña et al. [19] for DBS. Instead of performing a convex optimization as done in our study, Peña et al. [19] performed a particle swarm optimization and explicitly added the power consumption of the stimulation as an objective. To evaluate solutions for different weightings of the objectives, in our approach represented through the parameter λ, Peña et al. [19] computed a Pareto front. This approach has the advantage of directly obtaining optimal stimulation settings for different weightings of the objectives, but it leads to an increase in computation time. Whether this approach leads to advantages in practice is unclear, as an evaluation of this approach as well as a comparison of different optimization approaches in a simulation or patient study have yet to be performed.

4.3. Limitations

The design of this work as a retrospective study causes certain limitations regarding the significance of our results. For some models (mainly P3R and

P3L), our approach to determine the sensitivity parameter α led to optimization results that assigned high stimulation voltages to multiple contacts, which in turn led to a better stimulation of the VIM compared to the clinically determined monopolar stimulation (Fig. 2). In clinical practice, despite being below the voltage threshold at which side effects occur for each single contact, the optimization result might nevertheless lead to side effects, as the stimulation from the multiple contacts sums up. Therefore, in practice a smaller value for α might have to be chosen, which might diminish the theoretically computed improvement of the stimulation of the target region through the optimized stimulation settings (Fig. 2). However, also for a reduced value of α, the agreement between the clinically selected stimulation contacts and the optimization result, showing the predictive power of the optimization algorithm, persists. Actual improvements of the stimulation through the optimized stimulation settings cannot be shown in this retrospective design.

Whereas the motivation for the use of algorithms for an automatic determination of optimal DBS settings is the emerging use of leads with segmented contacts in clinical practice, the data utilized in this study were obtained for a quadripolar lead with cylindrical contacts. Thereby, the optimization problem (5) becomes less complex. Nevertheless, the reduced complexity does not affect the impact of our results, which prove that our choice of target and avoidance regions was adequate. On the contrary, the relatively simple programming of the quadripolar lead used for the patients in this study enabled the clinicians to select close to optimal stimulation settings. For more complex leads, we would expect an increased improvement through the use of the optimization algorithm compared to the one reported in Figure 2.

5. Outlook

The results of this retrospective study are an important indicator for the applicability of the optimization algorithm to automatically determine DBS settings in clinical practice. Whereas the results of this study validate the choice of target and avoidance regions for VIM DBS, similar studies have to be performed to determine the correct/necessary regions for other DBS targets, such as the subthalamic nucleus or the globus pallidus internus.

In future studies, the optimization algorithm should be applied during patient programming to evaluate whether the optimized settings lead to better treatment outcomes. The basic approach with which this can be performed is laid out in Section 2.7. The results of this study are promising with regard to the simplification of the programming of novel DBS leads with more than four contacts.

Conflicts of Interest

CRB has served as a consultant for NeuroPace, Advanced Bionics, Boston Scientific, IntelectMedical, Abbott (St. Jude Medical), and Functional Neuromodulation. CRB is also a shareholder of Intelect Medical and is an inventor

of several patents related to neuromodulation therapy. All other authors have nothing to declare.

Funding

This work was supported by the National Science Foundation (NSF): US IGNITE 10037840 under Dr. Christopher R. Butson and the Graduate Research Fellowship 1256065 under Daria Nesterovich Anderson. All data have been obtained within the Neuroscience Initiative project Functional Targeting for Deep Brain Stimulator Placement in Movement Disorders.

[1] G. Deuschl, C. Schade-Brittinger, P. Krack, J. Volkmann, H. Schäfer, K. Bötzel, C. Daniels, A. Deutschländer, U. Dillmann, W. Eisner, et al., A randomized trial of deep-brain stimulation for Parkinson's disease, New England Journal of Medicine 355 (9) (2006) 896–908.

[2] F. M. Weaver, K. Follett, M. Stern, K. Hur, C. Harris, W. J. Marks, J. Rothlind, O. Sagher, D. Reda, C. S. Moy, et al., Bilateral deep brain stimulation vs best medical therapy for patients with advanced Parkinson disease: a randomized controlled trial, Jama 301 (1) (2009) 63–73.

[3] A. L. Benabid, P. Pollak, D. Hoffmann, C. Gervason, M. Hommel, J. Perret, J. De Rougemont, D. Gao, Long-term suppression of tremor by chronic stimulation of the ventral intermediate thalamic nucleus, The Lancet 337 (8738) (1991) 403–406.

[4] W. Ondo, J. Jankovic, K. Schwartz, M. Almaguer, R. Simpson, Unilateral thalamic deep brain stimulation for refractory essential tremor and Parkinson's disease tremor, Neurology 51 (4) (1998) 1063–1069.

[5] W. C. Koller, K. E. Lyons, S. B. Wilkinson, A. I. Troster, R. Pahwa, Long-term safety and efficacy of unilateral deep brain stimulation of the thalamus in essential tremor, Movement disorders 16 (3) (2001) 464–468.

[6] K. Hunka, O. Suchowersky, S. Wood, L. Derwent, Z. H. Kiss, Nursing time to program and assess deep brain stimulators in movement disorder patients, Journal of Neuroscience Nursing 37 (4) (2005) 204.

[7] W. G. Ondo, H. Bronte-Stewart, The North American survey of placement and adjustment strategies for deep brain stimulation, Stereotactic and functional neurosurgery 83 (4) (2005) 142–147.

[8] G. Deli, I. Balas, F. Nagy, E. Balazs, J. Janszky, S. Komoly, N. Kovacs, Comparison of the efficacy of unipolar and bipolar electrode configuration during subthalamic deep brain stimulation, Parkinsonism & related disorders 17 (1) (2011) 50–54.

[9] J. Volkmann, E. Moro, R. Pahwa, Basic algorithms for the programming of deep brain stimulation in Parkinson's disease, Movement disorders: official journal of the Movement Disorder Society 21 (S14) (2006) S284–S289.

[10] J. Buhlmann, L. Hofmann, P. A. Tass, C. Hauptmann, Modeling of a segmented electrode for desynchronizing deep brain stimulation, Frontiers in neuroengineering 4 (2011) 15.

[11] J. Vitek, R. Jain, P. Starr, INTREPID Trial: A Prospective, Double blinded, Multi-center Randomized Controlled Trial Evaluating Deep Brain Stimulation with a New Multiple-Source, Constant-Current Rechargeable System in Parkinson's Disease (P5.016), Neurology 88 (16 Supplement), ISSN 0028-3878, URL `http://n.neurology.org/content/88/16_Supplement/P5.016`.

[12] M. F. Contarino, L. J. Bour, R. Verhagen, M. A. Lourens, R. M. de Bie, P. van den Munckhof, P. Schuurman, Directional steering A novel approach to deep brain stimulation, Neurology 83 (13) (2014) 1163–1169.

[13] C. Pollo, A. Kaelin-Lang, M. F. Oertel, L. Stieglitz, E. Taub, P. Fuhr, A. M. Lozano, A. Raabe, M. Schüpbach, Directional deep brain stimulation: an intraoperative double-blind pilot study, Brain 137 (7) (2014) 2015–2026.

[14] K. J. Van Dijk, R. Verhagen, A. Chaturvedi, C. C. McIntyre, L. J. Bour, C. Heida, P. H. Veltink, A novel lead design enables selective deep brain stimulation of neural populations in the subthalamic region, Journal of neural engineering 12 (4) (2015) 046003.

[15] A. Willsie, A. Dorval, Fabrication and initial testing of the μDBS: a novel Deep Brain Stimulation electrode with thousands of individually controllable contacts, Biomedical microdevices 17 (3) (2015) 56.

[16] R. Cubo, M. Åström, A. Medvedev, Electric field modeling and spatial control in Deep Brain Stimulation, in: Decision and Control (CDC), 2015 IEEE 54th Annual Conference on, IEEE, 3846–3851, 2015.

[17] R. Cubo, M. Åström, A. Medvedev, Optimization of lead design and electrode configuration in Deep Brain Stimulation, International Journal On Advances in Life Sciences 8 (2016) 76–86.

[18] Y. Xiao, E. Peña, M. D. Johnson, Theoretical optimization of stimulation strategies for a directionally segmented deep brain stimulation electrode array, IEEE Transactions on Biomedical Engineering 63 (2) (2016) 359–371.

[19] E. Peña, S. Zhang, S. Deyo, Y. Xiao, M. D. Johnson, Particle swarm optimization for programming deep brain stimulation arrays, Journal of neural engineering 14 (1) (2017) 016014.

[20] D. N. Anderson, B. Osting, J. Vorwerk, A. D. Dorval, C. R. Butson, Optimized programming algorithm for cylindrical and directional deep brain stimulation electrodes, Journal of neural engineering 15 (2) (2018) 026005.

[21] S. Mohammadi, H. E. Möller, H. Kugel, D. K. Müller, M. Deppe, Correcting eddy current and motion effects by affine whole-brain registrations: Evaluation of three-dimensional distortions and comparison with slicewise correction, Magnetic Resonance in Medicine 64 (4) (2010) 1047–1056.

[22] L. Ruthotto, H. Kugel, J. Olesch, B. Fischer, J. Modersitzki, M. Burger, C. Wolters, Diffeomorphic susceptibility artifact correction of diffusion-weighted magnetic resonance images, Physics in Medicine & Biology 57 (18) (2012) 5715.

[23] A. Krauth, R. Blanc, A. Poveda, D. Jeanmonod, A. Morel, G. Székely, A mean three-dimensional atlas of the human thalamus: generation from multiple histological data, Neuroimage 49 (3) (2010) 2053–2062.

[24] R. A. Bakay, chap. 11 Deep Brain Stimulation for Tremor, Georg Thieme Verlag, Stuttgart, ISBN 9781604060386, URL `http://www.thieme-connect.de/products/ebooks/lookinside/10.1055/b-0034-55961`, 2009.

[25] E. Papavassiliou, G. Rau, S. Heath, A. Abosch, N. M. Barbaro, P. S. Larson, K. Lamborn, P. A. Starr, Thalamic deep brain stimulation for essential tremor: relation of lead location to outcome, Neurosurgery 54 (5) (2004) 1120–1130.

[26] G. Grabner, A. L. Janke, M. M. Budge, D. Smith, J. Pruessner, D. L. Collins, Symmetric atlasing and model based segmentation: an application to the hippocampus in older adults, in: International Conference on Medical Image Computing and Computer-Assisted Intervention, Springer, 58–66, 2006.

[27] B. B. Avants, N. Tustison, G. Song, Advanced normalization tools (ANTS), Insight j 2 (2009) 1–35.

[28] H. Jiang, P. C. Van Zijl, J. Kim, G. D. Pearlson, S. Mori, DtiStudio: resource program for diffusion tensor computation and fiber bundle tracking, Computer methods and programs in biomedicine 81 (2) (2006) 106–116.

[29] C. R. Butson, C. C. McIntyre, Tissue and electrode capacitance reduce neural activation volumes during deep brain stimulation, Clinical neurophysiology 116 (10) (2005) 2490–2500.

[30] H. Si, TetGen, a Delaunay-based quality tetrahedral mesh generator, ACM Transactions on Mathematical Software (TOMS) 41 (2) (2015) 11.

[31] D. R. McNeal, Analysis of a model for excitation of myelinated nerve, IEEE Transactions on Biomedical Engineering (4) (1976) 329–337.

[32] F. Rattay, Analysis of models for external stimulation of axons, IEEE transactions on biomedical engineering (10) (1986) 974–977.

[33] E. N. Warman, W. M. Grill, D. Durand, Modeling the effects of electric fields on nerve fibers: determination of excitation thresholds, IEEE Transactions on Biomedical Engineering 39 (12) (1992) 1244–1254.

[34] C. C. McIntyre, S. Mori, D. L. Sherman, N. V. Thakor, J. L. Vitek, Electric field and stimulating influence generated by deep brain stimulation of the subthalamic nucleus, Clinical neurophysiology 115 (3) (2004) 589–595.

[35] C. R. Butson, C. C. McIntyre, Role of electrode design on the volume of tissue activated during deep brain stimulation, Journal of neural engineering 3 (1) (2005) 1.

[36] C. R. Butson, S. E. Cooper, J. M. Henderson, C. C. McIntyre, Patient-specific analysis of the volume of tissue activated during deep brain stimulation, Neuroimage 34 (2) (2007) 661–670.

[37] C. C. McIntyre, A. G. Richardson, W. M. Grill, Modeling the excitability of mammalian nerve fibers: influence of afterpotentials on the recovery cycle, Journal of neurophysiology 87 (2) (2002) 995–1006.

[38] A. Chaturvedi, C. R. Butson, S. F. Lempka, S. E. Cooper, C. C. McIntyre, Patient-specific models of deep brain stimulation: influence of field model complexity on neural activation predictions, Brain Stimulation: Basic, Translational, and Clinical Research in Neuromodulation 3 (2) (2010) 65–77.

[39] S. Wagner, M. Burger, C. H. Wolters, An optimization approach for well-targeted transcranial direct current stimulation, SIAM Journal on Applied Mathematics 76 (6) (2016) 2154–2174.